Covalently Functionalized Egyptian Blue Nanosheets for Near-Infrared Bioimaging

G. Selvaggio[1,2†], N. Herrmann[2†], B. Hill[1], R. Dervisoglu[3], S. Jung[1], M. Weitzel[2], M. Dinarvand[1,2], D. Stalke[4], L. Andreas[3], S. Kruss[1,2,5,6]

Fluorophores emitting in the near-infrared (NIR) wavelength region present optimal characteristics for photonics and especially bioimaging. Unfortunately, only few NIR fluorescent materials are known and even fewer are biocompatible. For this reason, the scientific interest in designing novel NIR fluorophores is very high. Egyptian Blue ($CaCuSi_4O_{10}$, EB) is a NIR fluorescent layered silicate that can be exfoliated into fluorescent nanosheets (EB-NS). So far, its surface chemistry has not been tailored but this is crucial for colloidal stability and biological targeting. Here, we demonstrate covalent surface functionalization of EB nanosheets (EBfunc) *via* Si-*H* activation using hydrosilanes with variable functionalities. EB-NS were first grafted with the visible fluorescent pyrene (Pyr) moieties to prove conjugation by colocalization of the Vis/NIR fluorescence on the (single) EB-NS level. The same procedure was performed and validated with carboxyl group (COOH)-containing hydrosilanes. These groups can serve as generic handle for further (bio)functionalization of the EB-NS surface. Finally, folic acid (FA) was conjugated to these COOH-functionalized EB-NS to target folic acid receptor-expressing cancer cells. These results highlight the potential of this surface chemistry approach to modify EB-NS and enable targeted NIR imaging for biomedical applications.

Introduction

After the discovery of graphene, two-dimensional (2D) nanomaterials have become an emerging class in science[1–3]. They provide numerous opportunities for electronics, catalysis, optics and (gas) storage on the nanoscale and beyond[1–9]. Furthermore, their use in biomedical applications is a main focus for researchers[10–15]. Classes of 2D nanomaterials which have proven successful in biomedicine include graphene, transition metal dichalcogenides (TMDs), layered double hydroxides (LDHs), silicate clays, transition metal oxides (TMOs), hexagonal boron nitride (hBN) and many more[16–18]. Hydrophobicity and the chemical inertness of most 2D nanomaterials are challenges especially for biological applications, in aqueous environments. Especially inorganic materials *e.g.* metal sulfides, chalcogenides and silicates require additional surface chemistry for example to guarantee colloidal stability. The tailoring of surface functionalization therefore plays a role of paramount importance for the achievement of enhanced colloidal stability, longer circulation times and improved biocompatibility. The possibility of decorating these nanomaterials with (bio)molecules of interest could furthermore allow therapeutic treatment, sensing and imaging applications[19].

Egyptian Blue ($CaCuSi_4O_{10}$, EB) is the most ancient pigment in the history of mankind, having its origins dated back to Ancient Egypt (≈ 2500 BC)[20,21]. This calcium copper tetrasilicate displays a layered crystal structure which allows to prepare nanosheets (NS) *via* simple stirring in hot water[22–27]. Most interestingly, it has been shown that the bright, stable and long-lived near-infrared (NIR) fluorescence of the bulk material (λ_{em} ≈ 910-930 nm)[25–30] is preserved in exfoliated NS down to just few tenths of nm in size[31,32]. The biocompatible nature of this class of layered silicates has been demonstrated by cell viability assays and *in vivo* studies[31]. Among them, an increasing number of publications has proven the high potential of EB-NS in the biomedical field as multi-functional platform for bioimaging[31,32], sensing[33], photothermal therapy (PTT)[34,35], tissue engineering[36,37] and more. Especially as novel NIR fluorophore, EB-NS appears of extreme interest. Fluorophores that emit in the NIR window (NIR-I: λ ≈ 750-1000 nm; NIR-II: λ ≈ 1000-1700 nm) present optimal characteristics for bioimaging due to reduced phototoxicity, scattering, absorption and autofluorescence of biological samples at these wavelengths[38–41]. Although organic dyes (*e.g.* indocyanine green[42], modified boron dipyrromethenes[43–46], *etc.*) and nanomaterials (*e.g.* quantum dots[47], silicon nanocrystals[48], single-walled carbon nanotubes[49–55], *etc.*) have been successfully implemented for numerous biological studies, their number is quite limited and in most cases they are affected by low quantum yield, low photostability and/or biocompatibility issues[40,42,47,56–59]. For these reasons, the interest in novel NIR materials is very high. Although the potential of EB-NS as NIR fluorophore has already been recognized [31,32], the next important step in this direction is tailoring of its surface chemistry. So far, the few publications which have described functionalization procedures on EB-NS have focused on lipophilic coatings. These were bond to the silicate surface either through electrostatic interactions (with *e.g.* the cationic surfactant cetyltrimethylammonium bromide, CTAB[60]) or covalently *via* silanization (with trimethylsilyl chloride, TMSCl[61,62]). Due to the non-covalent nature of the former, dynamics in the biological environment represent a challenge. The latter, on the other side, is covalent but also hydrophobic and inert, thus limited for biological applications.

1. *Department of Chemistry, Bochum University, Bochum, 44801, Germany.*
2. *Institute of Physical Chemistry, University of Göttingen, Göttingen, 37077, Germany.*
3. *Max-Planck-Institute for Multidisciplinary Sciences, Göttingen, 37077, Germany.*
4. *Institute of Inorganic Chemistry, University of Göttingen, Göttingen, 37077, Germany.*
5. *Fraunhofer Institute for Microelectronic Circuits and Systems, Duisburg, 47057, Germany.*
6. *Center for Nanointegration Duisburg-Essen (CENIDE).*

†*These authors contributed equally.*

**Corresponding author: sebastian.kruss@rub.de.*

Therefore, versatile chemical surface chemistry is crucial to use EB-NS *e.g.* for bioimaging.

Silicon-based nanoparticles (NPs) and materials have found several applications in the biomedical field[63–69]. These materials benefit from a well-established surface chemistry. For example, in the case of silica NPs, reactive functional moieties including the hydroxyl (-OH), carboxyl (-COOH), amine (-NH_2), azide (-N_3) and alkyl halogen groups can be covalently introduced either *via* co-condensation or by post-synthesis surface modification ("grafting"). While the former yields a more uniform distribution of functional groups, the latter does not significantly affect the size distribution and morphology of the silica NPs. The grafting procedure, which can be applied to diverse silica substrates, consists in the condensation of functionalized organosilicon compounds (typically silanes) with the accessible silanol groups (Si-OH) present on the surface of the silica-based material[70]. The most employed leaving groups in silanes are alkoxy groups (R_nSiX_{4-n}, X = OR'), but also alternatives such as halides, acyloxy and amino groups (X = halide, OCOR' and NR'_2 in R_nSiX_{4-n}) have been extensively reported. In this way, silane chemistry can robustly install strong bonds between the particle surface and (bio)molecules of interest, *e.g.* small organic molecules, fluorophores, nucleic acids, peptides, proteins, enzymes, antibodies, gold NPs, *etc.*[19,64–69]. However, the main issue with traditional alkoxy- (*e.g.* trialkoxysilane), halo- (*e.g.* chlorosilane), amino- (*e.g.* (3-aminopropyl)triethoxy silane, APTES) and acyloxysilanes coupling agents is that they are highly reactive and moisture sensitive, therefore purification steps can be challenging. A versatile alternative are hydrosilanes. These molecules are easily accessible, highly stable against moisture and allow simple purification. By choosing hydrosilanes as precursors and the strong Lewis acid tris(pentafluorophenyl)borane ($B(C_6F_5)_3$) as catalyst, *Moitra et al.*[71] have reported a promising method for surface modification of silica. This Si-*H* activation process, which has also later been adapted by *Sweetman et al.*[72] to porous silicon (pSi), can be performed at room temperature, is fast (reaction time ≈ 5 min), can be confirmed by naked eye (hydrogen release), and allows covalent binding of diverse groups.

In this work we report covalent functionalization of EB-NS *via* Si-*H* activation of hydrosilanes, followed by conjugation of EB-NS with different functional groups including folic acid (FA). We establish covalent (bio)functionalization of EB-NS and demonstrate targeted imaging of cancer cells **(Fig. 1)**.

Results

Functionalization (EBfunc) of Egyptian Blue Nanosheets (EB-NS) With Pyrene (Pyr)

Previous works have demonstrated that silanol groups are indeed accessible in significantly high numbers as a consequence of both synthesis and exfoliation procedures[22,35,73]. Our goal was to first demonstrate that this chemistry works in general and then to use it to bind biologically relevant molecules to EB-NS. To optimize the reaction conditions and to prove that this experimental procedure works on EB-NS, pyrene (Pyr) was chosen as the functional group (R). Its well-known fluorescence[74,75] acts as a visible control for the

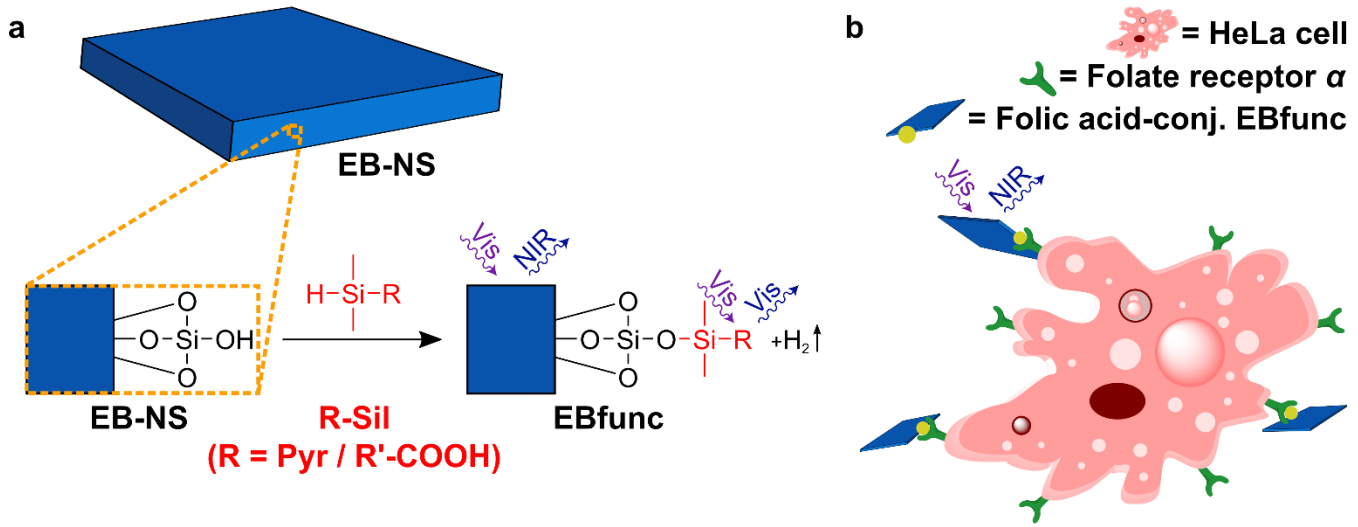

Figure 1: Surface functionalization of Egyptian Blue nanosheets for bioimaging. a *Procedure to graft hydrosilanes (R-Sil) onto the surface of Egyptian Blue nanosheets (EB-NS) via Si-H activation is illustrated. As R groups of the hydrosilanes, pyrene (Pyr) and an alkyl carboxylic acid for further conjugation were chosen. The NIR emission of EB-NS and the visible (Vis) fluorescence of Pyr are used to investigate the functionalization via colocalization. For clarity, only a small section of an EB-NS crystal with only one Si-OH on its surface is depicted.* ***b*** *EBfunc with folic acid (FA) is used to target and image FA receptors on cancer cells. Structures and objects are not to scale for better clarity.*

success of the grafting reaction. Therefore, 1-(dimethylsilyl)pyrene (Pyr-Sil) was synthesized from 1-bromopyrene and chlorodimethylsilane using a method known from literature[71] **(Fig. S1)**. The resulting silane was then reacted with EB-NS using $(C_6F_5)_3B$ as catalyst. The addition of the catalyst resulted in hydrogen evolution **(Fig. S2)**, as expected from the Si-*H* activation process and as reported in literature[71]. This observation represents a first visual indication that functionalization has been successful. After vigorous washing with dichloromethane (DCM) and hexane, the emission at visible wavelengths of the material (EBfunc) was investigated using fluorescence spectroscopy. The pyrene emission[76–78] was detected even after intense washing, thus excluding that only physisorption happened **(Fig. 2a)**. Without catalyst (noCAT) no visible fluorescence after the same washing procedure was observed, ruling out strong non-covalent binding between Pyr-Sil and EB-NS **(Fig. S3)**. Additionally, we examined whether the fluorescence of the visible- and NIR-emitting moieties (Pyr and EB-NS, respectively) changes. It is known that both radiative and non-radiative energy transfer between pyrene and other fluorescent molecules can happen if conditions such as close mutual distance and spectral overlap are met[75,79,80]. Interestingly, neither the Pyr **(Fig. 2a, Fig. S3)** nor the EB-NS **(Fig. 2b)** signals showed any significant difference compared to the starting materials[31,32]. This result shows that there is no energy transfer maybe because of the non-overlapping spectra. Nevertheless, the unchanged excitation and emission features of EB-NS once more underline the photostability of this silicate nanomaterial.

To prove functionalization on the single particle level and gain spatial information microscopy has to be used. The previously described EBfunc and noCAT powders were analyzed at a confocal laser scanning microscope (CLSM) to assess colocalization **(Fig. 3, Fig. S4-S5)**. With this method, successful functionalization can be deduced if the same particles are simultaneously observable in the bright field (BF) and in the visible fluorescence (PL) channel, meaning that fluorescent Pyr is present on the surface of the imaged nanostructure. EB-NS "as is" was chosen as one of the controls: considered that this represents pristine EB-NS which did not undergo any surface reaction and had thus no contact to pyrene, no fluorescence signal was expected here. Indeed, this control only yielded a very weak signal in the PL channel, likely determined by slight cross-talk of the CLSM optical path **(Fig. S5d,h)**. Analogously to the fluorescence spectroscopy dataset, the "noCAT" control sample was measured as well. In this case, the PL counts were slightly higher compared to the unprocessed EB-NS, yet the overall signal was very dim and colocalization was neglectable **(Fig. S5c,g)**. When measuring EBfunc, on the other side, a significantly stronger fluorescence intensity was observed over the entire sample. Furthermore, a high degree of colocalization could be measured for both larger and smaller NS structures **(Fig. 3, Fig. S5a,e)**. Indeed, the colocalization analysis indicated a comparable colocalization degree for the EB-NS and noCAT controls, whereas ≈ 2× higher values were calculated for EBfunc **(Fig. S5i)**. This dataset thus represents a further proof that Pyr is bound covalently in high number, while NS in the noCAT sample display at most a small amount of physisorbed pyrene.

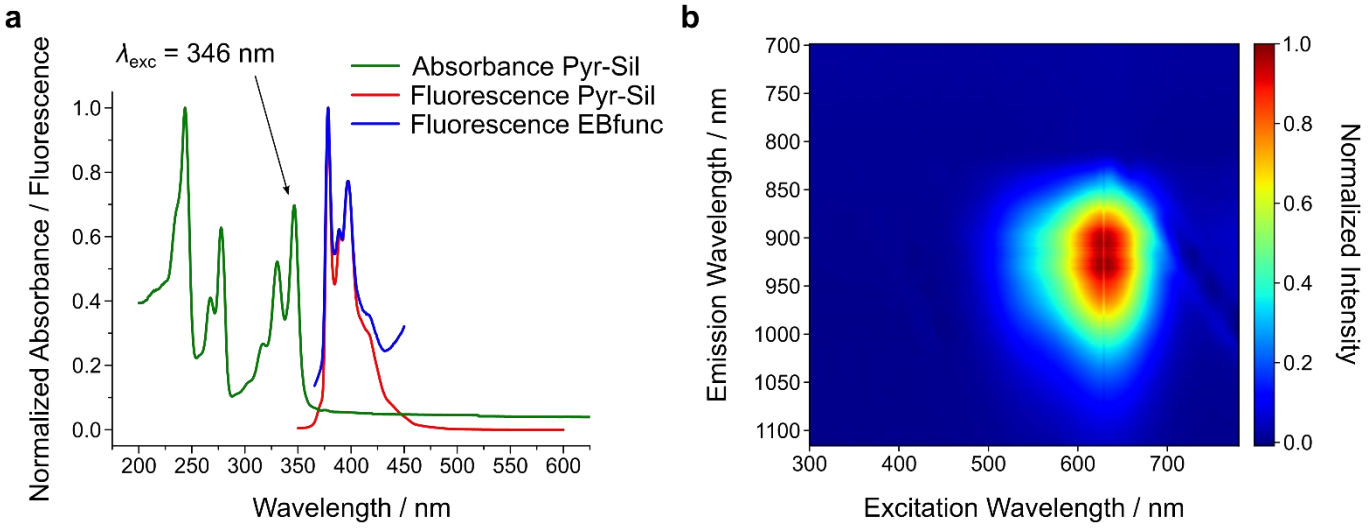

Figure 2: Proof of conjugation by absorbance and fluorescence spectroscopy. a *Pyrene has characteristic absorption features between 200-350 nm and fluorescence features between 370-400 nm which are observable in the synthesized 1-(dimethylsilyl)pyrene (Pyr-Sil). These emission features are also present in pyrene-functionalized EB-NS (EBfunc), even after several washing steps, which proves successful conjugation.* ***b*** *2D excitation-emission spectrum of EBfunc. It is not changed by the surface modification compared to EB-NS, thus highlighting on one side the robustness of EB-NS fluorescence, on the other side the absence of energy transfer between EB-NS and pyrene.*

In addition to the fluorescence studies described above, solid-state magic-angle spinning NMR analysis (MAS NMR) was performed on the previously defined EBfunc, noCAT and Pyr-Sil samples **(Fig. 4)**. Here, the signals of the 1-(dimethylsilyl)pyrene have been considered. We assigned the corresponding ^{13}C shifts of 0 ppm to the methyl and 120-140 ppm to the aromatic groups. EBfunc displayed a significant change of about +4 ppm in the chemical shift of the 0 ppm methyl groups. Furthermore, the aromatic peaks of Pyr-Sil were detected as well. Finally, no such signals were observed in the noCAT control. These findings directly prove attachment between the Si end of the Pyr-Sil and the Egyptian Blue surface. Hence, the ^{13}C MAS NMR data indicates a successful surface chemistry.

Functionalization (EBfunc) of Egyptian Blue Nanosheets (EB-NS) with Carboxyl Groups (COOH)

Next, we moved to more versatile reaction partners. 4-(dimethylsilyl)butanoic acid (COOH-Sil) was synthesized *via* a Grignard reaction from the corresponding chloro compound and carbon dioxide **(Fig. S6-S7)**. COOH-Sil was then added to EB-NS and the catalyst as previously described for Pyr-Sil, yielding in this case COOH-functionalized EB-NS (EBfunc). The grafting reaction led again to bubbling (*i.e.* hydrogen evolution), thus providing a first proof of successful covalent functionalization. When the reaction was repeated without the presence of the catalyst for the noCAT control sample, no bubbling could be observed. In a next step, after the usual washing and drying steps, zeta potential values of the EBfunc, noCAT and unprocessed EB-NS samples were measured **(Table 1)**. Acidic groups tend to dissociate in water at pH ≈ 7: although the surface of unmodified EB-NS is already negatively charged, we therefore expected the presence of carboxylic acid groups on EBfunc to further increase the amount of negative surface charges[31,81]. These can be robustly assessed *via* measurements of zeta potential, *i.e.* the electrical potential at the slipping plane of the investigated object. Indeed, the zeta potential of EBfunc (≈ -40 mV) decreased compared to noCAT and EB-NS (both ≈ -20 mV) suggesting the presence of grafted carboxyl groups on the surface of EBfunc. Furthermore, zeta potential is known to be a commonly employed tool to assess colloidal stability[82]. According to the well-established DVLO theory[83,84], the sum of van der Waals attractive and electrical double layer repulsive interactions between (nano)particles determines the

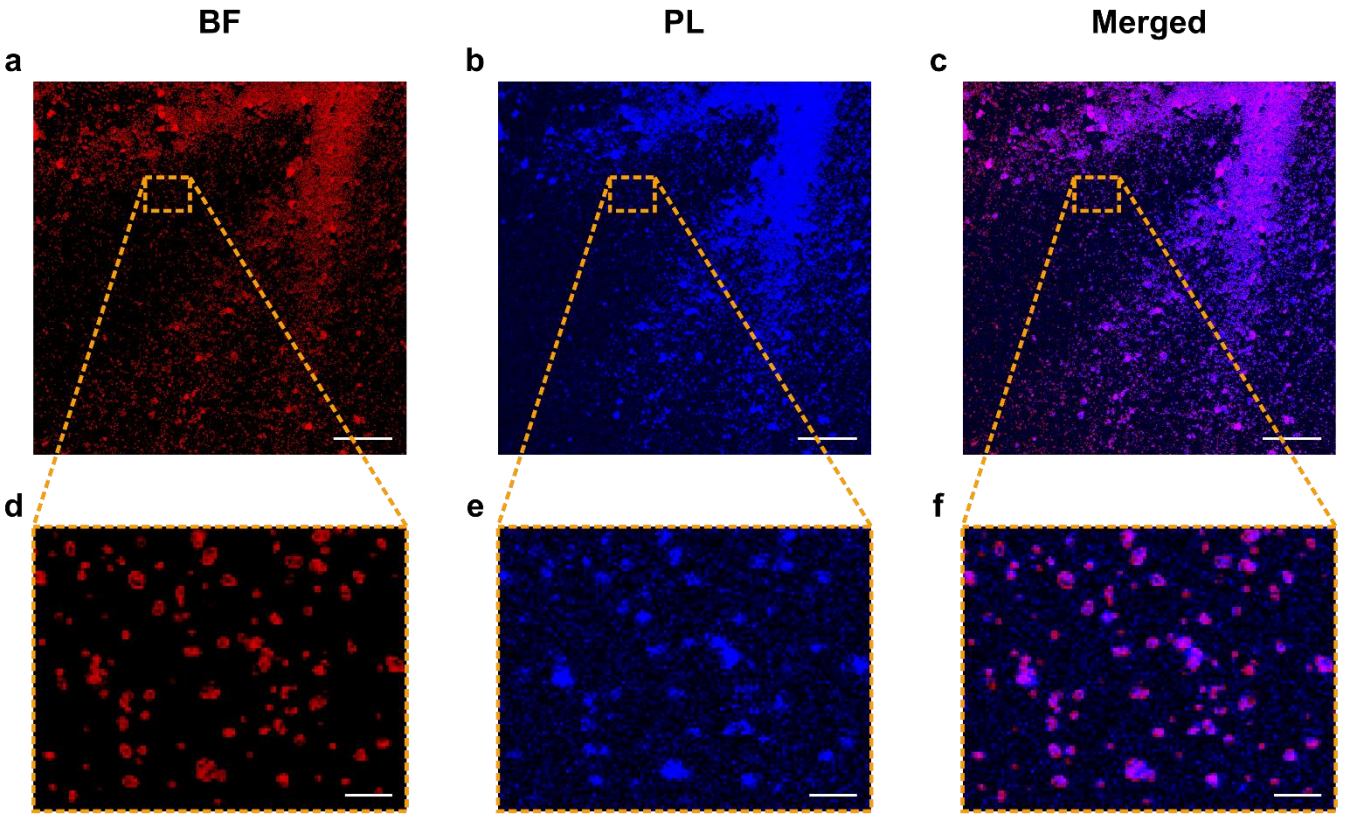

Figure 3: Proof of conjugation by optical colocalization. *Confocal laser scanning microscopy (CLSM) images of pyrene-functionalized EB-NS (EBfunc). The bright-field (BF,* ***a,d****), fluorescence (PL,* ***b,e****) and merged channels* ***(c,f)*** *of EBfunc imaged at a CLSM are shown. For both µm-sized and nm-sized EB-NS a high degree of colocalization is observed , which proves functionalization. Scale bar = 100 µm for overview images. Scale bar = 10 µm for blow-ups.*

stability of a colloidal system. In order for it to be stable and thus avoid the formation of aggregates, repulsive forces must prevail. Considered that the degree of particle repulsion is known to increase with higher absolute values of the zeta potential, this dataset also highlights a better colloidal stability of EBfunc. This lower tendency of agglomeration is of paramount importance for applications of these NS in biological systems.

***Table 1: Zeta potentials of EB-NS, COOH-functionalized EB-NS (EBfunc) and folic acid-conjugated EB-NS (FA-conjugated EBfunc)**. To verify the presence of carboxyl groups on the NS surface, zeta potential measurements on aliquots of EBfunc, the corresponding catalyst-free control sample (noCAT) and the unmodified EB-NS were performed. To confirm the conjugation of EBfunc with FA, zeta potential values of FA-conjugated EBfunc and the corresponding control were acquired. For both datasets, samples were dispersed in water and pH values were adjusted before measuring. N = 1 independent sample, n = 5 technical replicates.*

Sample	Zeta Potential ± Standard Deviation / mV	pH
EBfunc	-41 ± 2	6.83
noCAT	-21 ± 1	6.31
EB-NS	-20 ± 1	6.77
FA-conj. EBfunc	-38 ± 3	6.42
Control	-33 ± 2	6.11

Conjugation of Folic Acid (FA) onto COOH-Functionalized EB-NS (EBfunc)

With this functional carboxyl handle on the surface of EB-NS, classical conjugation chemistry can be used. Similar chemistries have been extensively performed for *e.g.* silica nanoparticles[19]. One interesting biomolecule is folic acid (vitamin B9, FA). This non-immunogenic, cost-efficient and stable molecule shows high affinity ($K_d \approx 0.1\text{-}1$ nM[85,86]) to the folate receptor (FR), which tends to be up-regulated in a wide range of human cancers. For this reason, tumor-specific treatments with high selectivity are envisioned, as demonstrated by the targeting of the most widely expressed isoform FRα by means of organic molecules, antibodies and nanoparticles[85–88]. Although the COOH group in the γ position on the FA core scaffold is most often used as handle for covalent attachment, other protocols exist which target amino groups instead, without compromising the binding strength of FA to FRα[86,89–92]. Inspired by one of these procedures[91], we therefore conjugated FA to COOH-functionalized EBfunc. As a control, the same reaction but without the addition of *N*,*N*′-dicyclohexylcarbodiimide (DCC) and *N*-hydroxysuccinimide (NHS) was repeated. The success of the conjugation protocol was first assessed by means of zeta potential **(Table 1)**: the more negative values for EBfunc compared to the control indicated a higher presence of negatively charged FA on the EBfunc surface. This outcome indicates successful conjugation beyond mere physisorption.

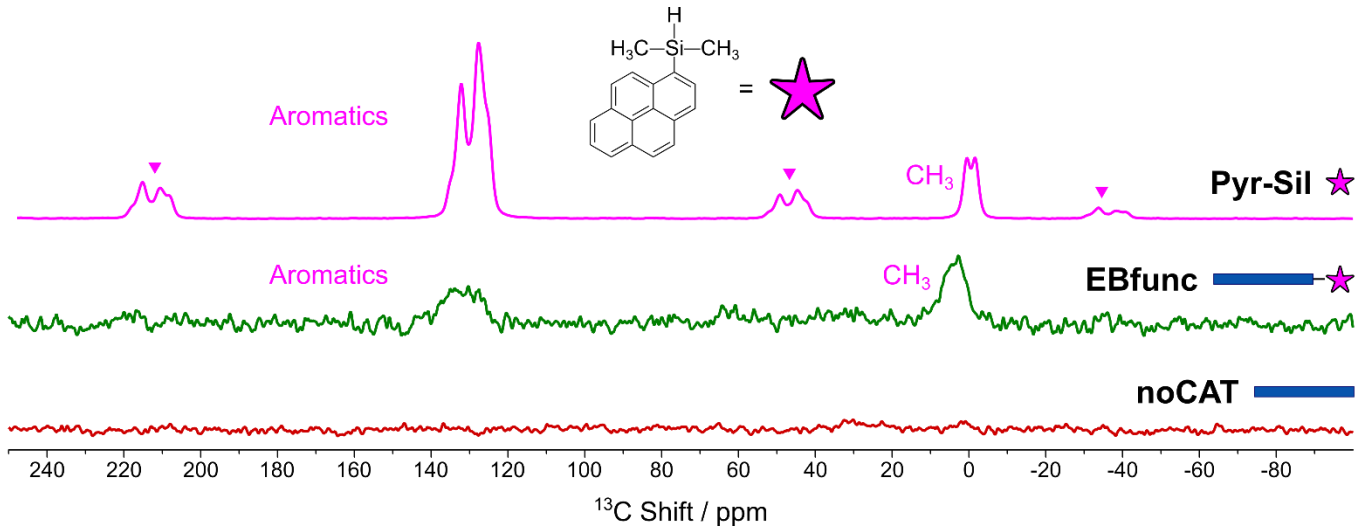

***Figure 4: Proof of conjugation by solid-state nuclear magnetic resonance (ssNMR).** ^{1}H-^{13}C cross-polarization (CP) magic-angle spinning (MAS) solid-state nuclear magnetic resonance (ssNMR) spectra of the 1-(dimethylsilyl)pyrene (Pyr-Sil), the pyrene-functionalized EB-NS (EBfunc) and the control sample without catalyst (noCAT) are reported. In Pyr-Sil, the peak at around 0 ppm belongs to the methyl groups attached to the Si atoms, whereas the 120-140 ppm peaks belong to the aromatic carbons of the pyrene moiety. Peaks denoted with triangles are spinning side bands. In EBfunc, the 4 ppm ^{13}C chemical shift belongs to the methyl groups and the 120-140 ppm to the aromatics from Pyr-Sil. The catalyst-free control sample shows no presence of the pyrene-silane either attached to the surface of EB-NS or free.*

Next, this novel FA-EBfunc conjugate was employed for tumor-selective targeting of HeLa cancer cells. These are epithelial cells from a cervical carcinoma which have been extensively used in biological studies and are known to express FRα in high amounts[85,89,91,93]. FA-conjugated EBfunc was introduced to these cell samples, which were then imaged at our home-built NIR microscopy setup. Here, colocalization experiments of the cells (phase contrast mode) and the FA-conjugated EBfunc (NIR fluorescence) were carried out **(Fig. 5)**. For the estimation of the degree of cell targeting displayed by FA-conjugated EBfunc, the positions of its NS relative to nearby cells were analyzed **(Fig. S8)**. In order to distinguish specific binding from simple physisorption, control EBfunc samples were prepared as mentioned above. Although non-specific binding events occurred, FA-conjugated EBfunc showed a higher degree of colocalization. This "background" looks different from the background one would expect from organic dyes because of the "particle" nature of EB-NS. It indicates a certain level of physisorption of non-functionalized EB-NS on cells. Nevertheless, this result suggests the presence of ligand-receptor binding events, which would be expected from the interaction between FA and the corresponding FRα receptors expressed by HeLa cells. In this way not only the conjugation chemistry performed on EBfunc was further confirmed, but the potential of functionalized EB-NS for bioimaging was also showcased.

Discussion

In this work a simple, robust and versatile protocol for the covalent functionalization of Egyptian Blue nanosheets (EB-NS) was described for the first time. The chosen approach, based on Si-*H* activation of hydrosilanes and adapted from the work of *Moitra et al.*[71], enables a large degree of freedom in terms of available R groups. We first demonstrated the applicability of this method on EB-NS by choosing a pyrene-bearing silane (Pyr-Sil) as precursor. A first proof of successful functionalization was given by hydrogen evolution, which could be easily observed by eye during the reaction. Next, we could exploit the visible fluorescence of pyrene to confirm its grafting onto the EB-NS surface *via* spectroscopic and imaging methods. As a final

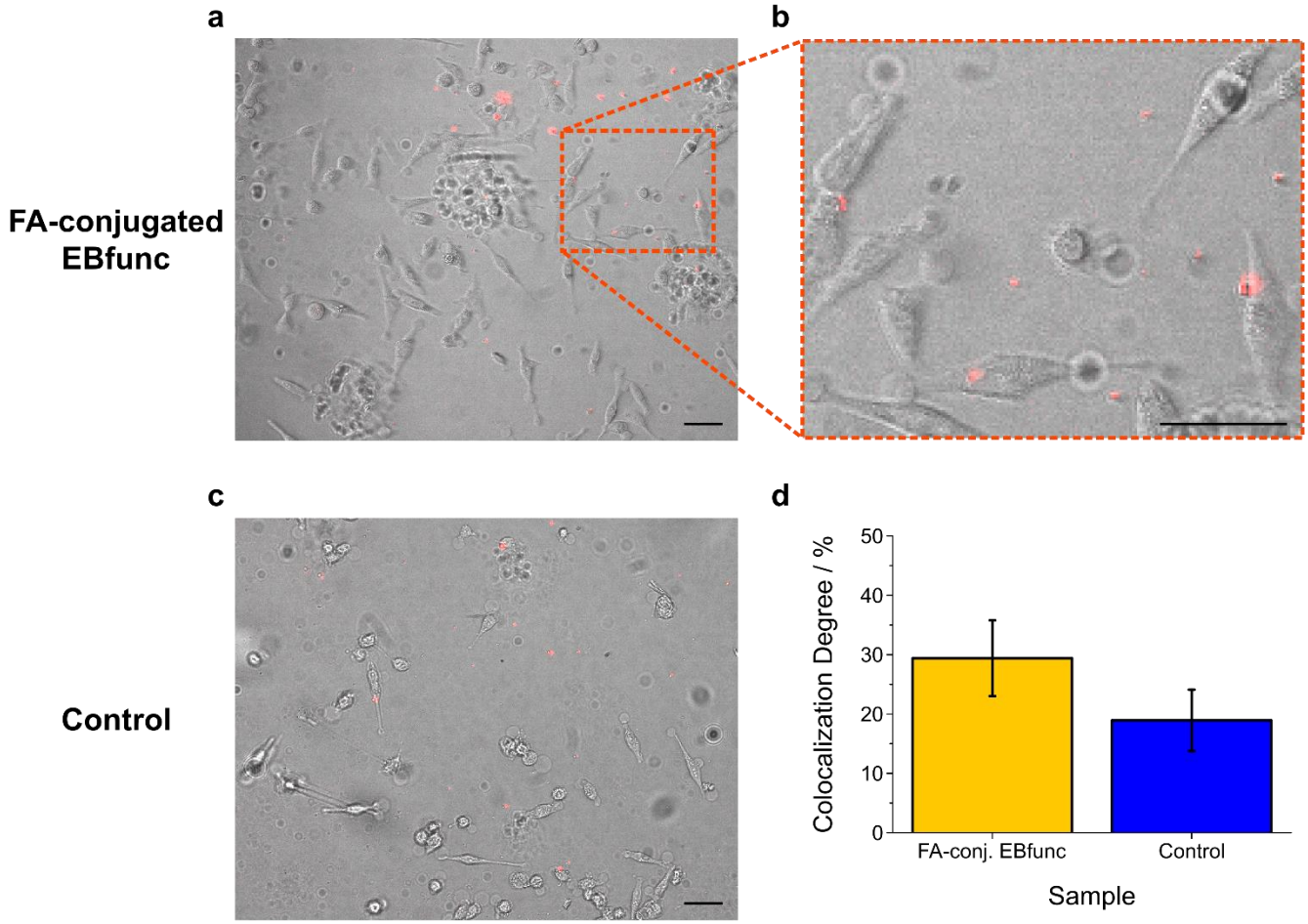

Figure 5: Targeted imaging of HeLa cells with folic acid (FA)-conjugated EBfunc. a-c *Exemplary merged microscopy images of HeLa cells (phase contrast, Vis channel, grayscale) incubated with FA-conjugated EBfunc* ***(a-b)*** *and EB-NS without FA* ***(c)*** *(fluorescence, NIR channel, red color). Scale bar = 50 µm.* ***d*** *The average colocalization highlights that EBfunc binds to a higher degree to FA expressing cells even though there is a background of non-specific adsorption. The cell labelling performance was evaluated by classifying NS particles according to their position relative to nearby cells. Data was normalized to the total number of NS present in the imaged region. Error bars = standard deviation. n = 4-5 analyzed regions of interest.*

characterization step, solid-state nuclear magnetic resonance (ssNMR) was chosen: by means of ^{1}H-^{13}C cross-polarization (CP) magic-angle spinning (MAS) measurements, the relevant signals of Pyr-Sil could be detected in the functionalized (EBfunc) sample. The versatility of this functionalization approach allowed us then to choose moieties of higher interest for *e.g.* bioimaging purposes. By following the same procedure, we explored the grafting reaction with a carboxylic acid-bearing silane (COOH-Sil). The covalent bonding of the carboxyl groups (COOH) onto the surface of EB-NS could be once more confirmed by the naked eye due to hydrogen evolution. Furthermore, zeta potential measurements clearly indicated an increased negative charge on the surface of COOH-functionalized EBfunc, which also led to an improved colloidal stability. Within the frame of biological applications, such features can result in *e.g.* an increased biocompatibility and a longer circulation time of EB *in vivo*. Finally, folic acid (FA) was linked to COOH-functionalized EBfunc *via* classical conjugation chemistry. This additional functionalization step, confirmed by zeta potential measurements, allowed NIR fluorescent labeling of cancer cells bearing folate receptors. Other NIR fluorescent nanomaterials such as SWCNTs have been successfully used for bioimaging and sensing[49,56]. A key to all these applications is versatile non-covalent and recently covalent surface chemistry[53,94,95]. It enabled imaging of neurotransmitters[96–100], reactive oxygen species[101–107], polyphenols[108], disease markers[33,53,109,110] and many other important analytes and biological targets. Translated to EB-NS, the versatile surface chemistry presented by us in this work will enable similar applications.

Conclusions

The NIR fluorescence of EB-NS offers many opportunities for biomedical applications and especially biophotonics. This work introduces a new covalent surface chemistry on EB-NS, which now provides access to numerous (bio)conjugation reactions for COOH-functionalized nanoparticles[19]. In combination with the highly promising chemical and photophysical properties of EB-NS[21], it represents an important step forward to establish EB-NS as robust and versatile fluorophore platform for NIR imaging.

Conflicts of Interest

The are no conflicts to declare.

Author Contributions

NH, GS and SK conceived and designed the study. SK coordinated the study. GS exfoliated EB into EB-NS. NH synthesized and characterized Pyr-Sil with support from GS. Corresponding NMR and MS data was analyzed by NH. NH and GS performed the grafting of Pyr-Sil onto EB-NS and acquired the 1D and 2D Vis-NIR spectroscopic dataset of pyrene-functionalized EBfunc. MD performed CLSM on pyrene-functionalized EBfunc samples prepared by GS and MW. Colocalization analysis of the CLSM dataset was performed by GS. ssNMR measurements were performed and analyzed by RD and LA with support from NH. GS synthesized COOH-preSil and COOH-Sil with support from DS, NH and MW. Corresponding NMR and MS data was analyzed by NH. The grafting of COOH-Sil onto EB-NS to yield COOH-functionalized EBfunc was performed by GS with support from DS and NH. BH acquired zeta potential measurements on COOH-functionalized EBfunc. BH and SJ carried out FA conjugation and cell experiments with support from GS. GS, NH and SK wrote the manuscript, with contributions from all authors.

Acknowledgments

This work was funded by the Deutsche Forschungsgemeinschaft (DFG, German Research Foundation) under Germany's Excellence Strategy—EXC 2033–390677874—RESOLV. This work was further supported by the "Center for Solvation Science ZEMOS" funded by the German Federal Ministry of Education and Research BMBF and by the Ministry of Culture and Research of Nord Rhine-Westphalia. We would also like to acknowledge support from the VW Foundation. We are grateful to Dr. Volker Karius and Cornelia Friedrich for granting access to their labs and for expert technical assistance. We also thank Prof. Steinem and Prof. Janshoff for support. We are also thankful to Jutta Gerber-Nolte, Angela Rübeling and all other members of the research groups of Prof. Steinem and Prof. Janshoff for the constant support. We are grateful to Laura Haberstock, Tobias Ernemann, Daniel Lüert, Tobias Heitkemper and Xiaobai Wang for providing equipment and technical assistance for synthetic chemistry. We are grateful to Niyaz Alizadeh, Dr. Antonio Del Vecchio, Dr. Fabio Pesciaioli and Dr. Leonardo Massignan for the fruitful discussions and their expert technical assistance. We also thank Dr. Lena Schnitzler, Dr. Linda Sistemich, Justus Metternich and Alexander Schrage for the fruitful discussions and technical support.

References

1 A. K. Geim and K. S. Novoselov, The rise of graphene, *Nat. Mater.*, 2007, **6**, 183–191, 10.1038/nmat1849.

2 A. K. Geim, Graphene: Status and Prospects, *Science*, 2009, **324**, 1530–1534, 10.1126/science.1158877.

3 K. S. Novoselov, A. K. Geim, S. V Morozov, D. Jiang, Y. Zhang, S. V Dubonos, I. V Grigorieva and A. A. Firsov, Electric Field Effect in Atomically Thin Carbon Films, *Science*, 2004, **306**, 666–669, 10.1126/science.1102896.

4 V. Nicolosi, M. Chhowalla, M. G. Kanatzidis, M. S. Strano and J. N. Coleman, Liquid exfoliation of layered materials, *Science*, 2013, **340**, 72–75, 10.1126/science.1226419.

5 K. S. Novoselov, D. Jiang, F. Schedin, T. J. Booth, V. V. Khotkevich, S. V. Morozov and A. K. Geim, Two-dimensional atomic crystals, *Proc. Natl. Acad. Sci. U. S. A.*, 2005, **102**, 10451–10453, 10.1073/pnas.0502848102.

6 Q. H. Wang, K. Kalantar-Zadeh, A. Kis, J. N. Coleman and M. S. Strano, Electronics and optoelectronics of two-dimensional transition metal dichalcogenides, *Nat. Nanotechnol.*, 2012, **7**, 699–712, 10.1038/nnano.2012.193.

7 H. Tao, Y. Zhang, Y. Gao, Z. Sun, C. Yan and J. Texter, Scalable exfoliation and dispersion of two-dimensional materials-an update, *Phys. Chem. Chem. Phys.*, 2017, **19**, 921–960, 10.1039/c6cp06813h.

8 A. Kumar and C. Huei, Synthesis and Biomedical Applications of Graphene: Present and Future Trends, in *Advances in Graphene Science*, InTech, 2013, 10.5772/55728.

9 G. R. Bhimanapati, Z. Lin, V. Meunier, Y. Jung, J. Cha, S. Das, D. Xiao, Y. Son, M. S. Strano, V. R. Cooper, L. Liang, S. G. Louie, E. Ringe, W. Zhou, S. S. Kim, R. R. Naik, B. G. Sumpter, H. Terrones, F. Xia, Y. Wang, J. Zhu, D. Akinwande, N. Alem, J. A. Schuller, R. E. Schaak, M. Terrones and J. A. Robinson, Recent Advances in Two-Dimensional Materials beyond Graphene, *ACS Nano*, 2015, **9**, 11509–11539, 10.1021/acsnano.5b05556.

10 W. J. Parak, D. Gerion, D. Zanchet, A. S. Woerz, T. Pellegrino, C. Micheel, S. C. Williams, M. Seitz, R. E. Bruehl, Z. Bryant, C. Bustamante, C. R. Bertozzi and A. P. Alivisatos, Conjugation of DNA to silanized colloidal semiconductor nanocrystalline quantum dots, *Chem. Mater.*, 2002, **14**, 2113–2119, 10.1021/cm0107878.

11 B. Pelaz, C. Alexiou, R. A. Alvarez-Puebla, F. Alves, A. M. Andrews, S. Ashraf, L. P. Balogh, L. Ballerini, A. Bestetti, C. Brendel, S. Bosi, M. Carril, W. C. W. Chan, C. Chen, X. X. Chen, X. X. Chen, Z. Cheng, D. Cui, J. Du, C. Dullin, A. Escudero, N. Feliu, M. Gao, M. George, Y. Gogotsi, A. Grünweller, Z. Gu, N. J. Halas, N. Hampp, R. K. Hartmann, M. C. Hersam, P. Hunziker, J. Jian, X. Jiang, P. Jungebluth, P. Kadhiresan, K. Kataoka, A. Khademhosseini, J. Kopeček, N. A. Kotov, H. F. Krug, D. S. Lee, C. M. Lehr, K. W. Leong, X. J. Liang, M. L. Lim, L. M. Liz-Marzán, X. Ma, P. Macchiarini, H. Meng, H. Möhwald, P. Mulvaney, A. E. Nel, S. Nie, P. Nordlander, T. Okano, J. Oliveira, T. H. Park, R. M. Penner, M. Prato, V. Puntes, V. M. Rotello, A. Samarakoon, R. E. Schaak, Y. Shen, S. Sjöqvist, A. G. Skirtach, M. G. Soliman, M. M. Stevens, H. W. Sung, B. Z. Tang, R. Tietze, B. N. Udugama, J. Scott VanEpps, T. Weil, P. S. Weiss, I. Willner, Y. Wu, L. Yang, Z. Yue, Q. Zhang, Q. Zhang, X. E. Zhang, Y. Zhao, X. Zhou and W. J. Parak, Diverse Applications of Nanomedicine, *ACS Nano*, 2017, **11**, 2313–2381, 10.1021/acsnano.6b06040.

12 M. V. Kovalenko, L. Manna, A. Cabot, Z. Hens, D. V. Talapin, C. R. Kagan, V. I. Klimov, A. L. Rogach, P. Reiss, D. J. Milliron, P. Guyot-Sionnnest, G. Konstantatos, W. J. Parak, T. Hyeon, B. A. Korgel, C. B. Murray and W. Heiss, Prospects of nanoscience with nanocrystals, *ACS Nano*, 2015, **9**, 1012–1057, 10.1021/nn506223h.

13 A. C. Ferrari, F. Bonaccorso, V. Fal'ko, K. S. Novoselov, S. Roche, P. Bøggild, S. Borini, F. H. L. Koppens, V. Palermo, N. Pugno, J. A. Garrido, R. Sordan, A. Bianco, L. Ballerini, M. Prato, E. Lidorikis, J. Kivioja, C. Marinelli, T. Ryhänen, A. Morpurgo, J. N. Coleman, V. Nicolosi, L. Colombo, A. Fert, M. Garcia-Hernandez, A. Bachtold, G. F. Schneider, F. Guinea, C. Dekker, M. Barbone, Z. Sun, C. Galiotis, A. N. Grigorenko, G. Konstantatos, A. Kis, M. Katsnelson, L. Vandersypen, A. Loiseau, V. Morandi, D. Neumaier, E. Treossi, V. Pellegrini, M. Polini, A. Tredicucci, G. M. Williams, B. Hee Hong, J. H. Ahn, J. Min Kim, H. Zirath, B. J. Van Wees, H. Van Der Zant, L. Occhipinti, A. Di Matteo, I. A. Kinloch, T. Seyller, E. Quesnel, X. Feng, K. Teo, N. Rupesinghe, P. Hakonen, S. R. T. Neil, Q. Tannock, T. Löfwander and J. Kinaret, Science and technology roadmap for graphene, related two-dimensional crystals, and hybrid systems, *Nanoscale*, 2015, **7**, 4598–4810, 10.1039/c4nr01600a.

14 C. Martín, K. Kostarelos, M. Prato and A. Bianco, Biocompatibility and biodegradability of 2D materials: Graphene and beyond, *Chem. Commun.*, 2019, **55**, 5540–5546, 10.1039/c9cc01205b.

15 G. Reina, J. M. González-Domínguez, A. Criado, E. Vázquez, A. Bianco and M. Prato, Promises, facts and challenges for graphene in biomedical applications, *Chem. Soc. Rev.*, 2017, **46**, 4400–4416, 10.1039/c7cs00363c.

16 D. Chimene, D. L. Alge and A. K. Gaharwar, Two-Dimensional Nanomaterials for Biomedical Applications: Emerging Trends and Future Prospects, *Adv. Mater.*, 2015, **27**, 7261–7284, 10.1002/adma.201502422.

17 T. Hu, X. Mei, Y. Wang, X. Weng, R. Liang and M. Wei, Two-dimensional nanomaterials: fascinating materials in biomedical field, *Sci. Bull.*, 2019, **64**, 1707–1727,

10.1016/j.scib.2019.09.021.

18 M. Derakhshi, S. Daemi, P. Shahini, A. Habibzadeh, E. Mostafavi and A. A. Ashkarran, Two-Dimensional Nanomaterials beyond Graphene for Biomedical Applications, *J. Funct. Biomater.*, 2022, **13**, 27, 10.3390/jfb13010027.

19 V. Biju, Chemical modifications and bioconjugate reactions of nanomaterials for sensing, imaging, drug delivery and therapy, *Chem. Soc. Rev.*, 2014, **43**, 744–764, 10.1039/c3cs60273g.

20 A. Sgamellotti and C. Anselmi, An evergreen blue. Spectroscopic properties of Egyptian blue from pyramids to Raphael, and beyond, *Inorganica Chim. Acta*, 2022, **530**, 120699, 10.1016/j.ica.2021.120699.

21 G. Selvaggio and S. Kruss, Preparation, properties and applications of near-infrared fluorescent silicate nanosheets, *Nanoscale*, , DOI:10.1039/D2NR02967G, 10.1039/D2NR02967G.

22 T. E. Warner, *Synthesis, Properties and Mineralogy of Important Inorganic Materials*, *Synthesis, Properties and Mineralogy of Important Inorganic Materials*, Wiley, Chichester, UK, 2011, 10.1002/9780470976012.

23 A. Pabst, Structures of some tetragonal sheet silicates, *Acta Crystallogr.*, 1959, **12**, 733–739, 10.1107/s0365110x5900216x.

24 B. C. Chakoumakos, J. A. Fernandez-Baca and L. A. Boatner, Refinement of the Structures of the Layer Silicates MCuSi4O10 (M = Ca, Sr, Ba) by Rietveld Analysis of Neutron Powder Diffraction Data, *J. Solid State Chem.*, 1993, **103**, 105–113.

25 D. Johnson-Mcdaniel, C. A. Barrett, A. Sharafi and T. T. Salguero, Nanoscience of an Ancient Pigment, *J. Am. Chem. Soc.*, 2013, **135**, 1677–1679, 10.1021/ja310587c.

26 D. Johnson-McDaniel and T. T. Salguero, Exfoliation of Egyptian Blue and Han Blue, Two Alkali Earth Copper Silicate-based Pigments, *J. Vis. Exp.*, 2014, 1–10.

27 T. T. Salguero, D. Johnson-McDaniel, C. A. Barrett, A. Sharafi, R. Weimar and T. Blevins, Nanoscience of Metal Silicate-Based Pigments, *MRS Proc.*, 2014, **1618**, 161–166, 10.1557/opl.2014.465.

28 G. Pozza, D. Ajò, G. Chiari, F. De Zuane and M. Favaro, Photoluminescence of the inorganic pigments Egyptian blue, Han blue and Han purple, *J. Cult. Herit.*, 2000, **1**, 393–398, 10.1016/S1296-2074(00)01095-5.

29 D. Ajò, G. Chiari, F. De Zuane, M. Favaro and M. Bertolin, Photoluminescence of some blue natural pigments and related synthetic materials, *5th Int. Conf. non-destructive testing, Microanal. methods Environ. Eval. study Conserv. Work. art*, 1996, 37–47.

30 G. Accorsi, G. Verri, M. Bolognesi, N. Armaroli, C. Clementi, C. Miliani and A. Romani, The exceptional near-infrared luminescence properties of cuprorivaite (Egyptian blue), *Chem. Commun.*, 2009, 3392–3394.

31 G. Selvaggio, A. Chizhik, R. Nißler, L. Kuhlemann, D. Meyer, L. Vuong, H. Preiß, N. Herrmann, F. A. Mann, Z. Lv, T. A. Oswald, A. Spreinat, L. Erpenbeck, J. Großhans, V. Karius, A. Janshoff, J. Pablo Giraldo and S. Kruss, Exfoliated near infrared fluorescent silicate nanosheets for (bio)photonics, *Nat. Commun.*, 2020, **11**, 1495, 10.1038/s41467-020-15299-5.

32 G. Selvaggio, M. Weitzel, N. Oleksiievets, T. A. Oswald, R. Nißler, I. Mey, V. Karius, J. Enderlein, R. Tsukanov and S. Kruss, Photophysical properties and fluorescence lifetime imaging of exfoliated near-infrared fluorescent silicate nanosheets, *Nanoscale Adv.*, 2021, **3**, 4541–4553, 10.1039/d1na00238d.

33 R. Nißler, O. Bader, M. Dohmen, S. G. Walter, C. Noll, G. Selvaggio, U. Groß and S. Kruss, Remote near infrared identification of pathogens with multiplexed nanosensors, *Nat. Commun.*, 2020, **11**, 5995, 10.1038/s41467-020-19718-5.

34 C. He, C. Dong, L. Yu, Y. Chen and Y. Hao, Ultrathin 2D Inorganic Ancient Pigment Decorated 3D-Printing Scaffold Enables Photonic Hyperthermia of Osteosarcoma in NIR-II Biowindow and Concurrently Augments Bone Regeneration, *Adv. Sci.*, 2021, **8**, 1–10, 10.1002/advs.202101739.

35 Q. Yu, Y. Han, T. Tian, Q. Zhou, Z. Yi, J. Chang and C. Wu, Chinese sesame stick-inspired nano-fibrous scaffolds for tumor therapy and skin tissue reconstruction, *Biomaterials*, 2019, **194**, 25–35, 10.1016/j.biomaterials.2018.12.012.

36 C. Yang, R. Zheng, M. R. Younis, J. Shao, L.-H. Fu, D.-Y. Zhang, J. Lin, Z. Li and P. Huang, NIR-II light-responsive biodegradable shape memory composites based on cuprorivaite nanosheets for enhanced tissue reconstruction, *Chem. Eng. J.*, 2021, **419**, 129437, 10.1016/j.cej.2021.129437.

37 C. Dong, C. Yang, M. R. Younis, J. Zhang, G. He, X. Qiu, L. Fu, D. Zhang, H. Wang, W. Hong, J. Lin, X. Wu and P. Huang, Bioactive NIR-II Light-Responsive Shape Memory Composite Based on Cuprorivaite Nanosheets for Endometrial Regeneration, *Adv. Sci.*, 2022, **2102220**, 2102220, 10.1002/advs.202102220.

38 A. M. Smith, M. C. Mancini and S. Nie, Second window for in vivo imaging, *Nat. Nanotechnol.*, 2009, **4**, 710–711, 10.1038/nnano.2009.326.

39 E. A. Owens, M. Henary, G. El Fakhri and H. S. Choi, Tissue-Specific Near-Infrared Fluorescence Imaging, *Acc. Chem. Res.*, 2016, **49**, 1731–1740, 10.1021/acs.accounts.6b00239.

40 G. Hong, A. L. Antaris and H. Dai, Near-infrared fluorophores for biomedical imaging, *Nat. Biomed. Eng.*, 2017, **1**, 1–9, 10.1038/s41551-016-0010.

41 A. Spreinat, G. Selvaggio, L. Erpenbeck and S. Kruss, Multispectral near infrared absorption imaging for histology of skin cancer, *J. Biophotonics*, 2020, **13**, e201960080, 10.1002/JBIO.201960080.

42 J. A. Carr, D. Franke, J. R. Caram, C. F. Perkinson, M. Saif, V. Askoxylakis, M. Datta, D. Fukumura, R. K. Jain, M. G. Bawendi and O. T. Bruns, Shortwave infrared fluorescence imaging with the clinically approved near-infrared dye indocyanine green., *Proc. Natl. Acad. Sci. U. S. A.*, 2018, **115**, 4465–4470, 10.1073/pnas.1718917115.

43 A. Loudet and K. Burgess, BODIPY dyes and their derivatives: Syntheses and spectroscopic properties, *Chem. Rev.*, 2007, **107**, 4891–4932, 10.1021/cr078381n.

44 G. Ulrich, R. Ziessel and A. Harriman, The chemistry of fluorescent bodipy dyes: Versatility unsurpassed, *Angew. Chemie - Int. Ed.*, 2008, **47**, 1184–1201, 10.1002/anie.200702070.

45 A. Patra, L. J. Patalag, P. G. Jones and D. B. Werz, Extended Benzene-Fused Oligo-BODIPYs: In Three Steps to a Series of Large, Arc-Shaped, Near-Infrared Dyes, *Angew. Chemie - Int. Ed.*, 2021, **60**, 747–752, 10.1002/anie.202012335.

46 G. Selvaggio, R. Nißler, P. Nietmann, A. Patra, L. J. Patalag, A. Janshoff, D. B. Werz and S. Kruss, NIR-emitting benzene-fused oligo-BODIPYs for bioimaging, *Analyst*, 2022, **147**, 230–237, 10.1039/D1AN01850G.

47 O. T. Bruns, T. S. Bischof, D. K. Harris, D. Franke, Y. Shi, L. Riedemann, A. Bartelt, F. B. Jaworski, J. A. Carr, C. J. Rowlands, M. W. B. B. Wilson, O. Chen, H. Wei, G. W. Hwang, D. M. Montana, I. Coropceanu, O. B. Achorn, J. Kloepper, J. Heeren, P. T. C. C. So, D. Fukumura, K. F. Jensen, R. K. Jain and M. G. Bawendi, Next-generation in vivo optical imaging with short-wave infrared quantum dots, *Nat. Biomed. Eng.*, 2017, **1**, 0056, 10.1038/s41551-017-0056.

48 F. Romano, S. Angeloni, G. Morselli, R. Mazzaro, V. Morandi, J. R. Shell, X. Cao, B. W. Pogue and P. Ceroni, Water-soluble silicon nanocrystals as NIR luminescent probes for time-gated biomedical imaging, *Nanoscale*, 2020, **12**, 7921–7926, 10.1039/D0NR00814A.

49 J. Ackermann, J. T. Metternich, S. Herbertz and S. Kruss, Biosensing with Fluorescent Carbon Nanotubes, *Angew. Chemie - Int. Ed.*, 2022, **61**, e202112372, 10.1002/anie.202112372.

50 S. Kruss, A. J. Hilmer, J. Zhang, N. F. Reuel, B. Mu and M. S. Strano, Carbon nanotubes as optical biomedical sensors, *Adv. Drug Deliv. Rev.*, 2013, **65**, 1933–1950, 10.1016/j.addr.2013.07.015.

51 G. Bisker, J. Dong, H. D. Park, N. M. Iverson, J. Ahn, J. T. Nelson, M. P. Landry, S. Kruss and M. S. Strano, Protein-targeted corona phase molecular recognition, *Nat. Commun.*, 2016, **7**, 1–14, 10.1038/ncomms10241.

52 J. P. Giraldo, H. Wu, G. M. Newkirk and S. Kruss, Nanobiotechnology approaches for engineering smart plant sensors, *Nat. Nanotechnol.*, 2019, **14**, 541–553, 10.1038/s41565-019-0470-6.

53 M. Kim, C. Chen, P. Wang, J. J. Mulvey, Y. Yang, C. Wun, M. Antman-Passig, H.-B. Luo, S. Cho, K. Long-Roche, L. V. Ramanathan, A. Jagota, M. Zheng, Y. Wang and D. A. Heller, Detection of ovarian cancer via the spectral fingerprinting of quantum-defect-modified carbon nanotubes in serum by machine learning, *Nat. Biomed. Eng.*, 2022, **6**, 267–275, 10.1038/s41551-022-00860-y.

54 A. Antonucci, J. Kupis-Rozmysłowicz and A. A. Boghossian, Noncovalent Protein and Peptide Functionalization of Single-Walled Carbon Nanotubes for Biodelivery and Optical Sensing Applications, *ACS Appl. Mater. Interfaces*, 2017, **9**, 11321–11331, 10.1021/acsami.7b00810.

55 N. E. Kallmyer, M. S. Abdennadher, S. Agarwal, R. Baldwin-Kordick, R. L. Khor, A. S. Kooistra, E. Peterson, M. D. McDaniel and N. F. Reuel, Inexpensive Near-Infrared Fluorimeters: Enabling Translation of nIR-Based Assays to the Field, *Anal. Chem.*, 2021, **93**, 4800–4808, 10.1021/acs.analchem.0c03732.

56 G. Hong, S. Diao, A. L. Antaris and H. Dai, Carbon Nanomaterials for Biological Imaging and Nanomedicinal Therapy, *Chem. Rev.*, 2015, **115**, 10816–10906, 10.1021/acs.chemrev.5b00008.

57 S. He, J. Song, J. Qu and Z. Cheng, Crucial breakthrough of second near-infrared biological window fluorophores: design and synthesis toward multimodal imaging and theranostics, *Chem. Soc. Rev.*, 2018, **47**, 4258–4278, 10.1039/C8CS00234G.

58 Z. Lei and F. Zhang, Molecular Engineering of NIR-II Fluorophores for Improved Biomedical Detection, *Angew. Chemie - Int. Ed.*, 2021, **60**, 16294–16308, 10.1002/anie.202007040.

59 Y. Fan, P. Wang, Y. Lu, R. Wang, L. Zhou, X. Zheng, X. Li, J. A. Piper and F. Zhang, Lifetime-engineered NIR-II nanoparticles unlock multiplexed in vivo imaging, *Nat. Nanotechnol.*, 2018, **13**, 941–946, 10.1038/s41565-018-0221-0.

60 S. Shahbazi, J. V. Goodpaster, G. D. Smith, T. Becker and S. W. Lewis, Preparation, characterization, and application of a lipophilic coated exfoliated Egyptian blue for near-infrared luminescent latent fingermark detection, *Forensic Chem.*, 2020, **18**, 100208, 10.1016/j.forc.2019.100208.

61 S. M. Borisov, C. Würth, U. Resch-Genger and I. Klimant, New Life of Ancient Pigments: Application in High-Performance Optical Sensing Materials, *Anal. Chem.*, 2013, **85**, 9371–9377, 10.1021/ac402275g.

62 M. Maierhofer, V. Rieger and T. Mayr, Optical ammonia sensors based on fluorescent aza-BODIPY dyes— a flexible toolbox, *Anal. Bioanal. Chem.*, 2020, **412**, 7559–7567, 10.1007/s00216-020-02891-3.

63 L. Ma, X. Song, Y. Yu and Y. Chen, Two-Dimensional Silicene/Silicon Nanosheets: An Emerging Silicon-Composed Nanostructure in Biomedicine, *Adv. Mater.*, 2021, **33**, 2008226, 10.1002/adma.202008226.

64 K. Wang, X. He, X. Yang and H. Shi, Functionalized silica nanoparticles: A platform for fluorescence imaging at the cell and small animal levels, *Acc. Chem. Res.*, 2013, **46**, 1367–1376, 10.1021/ar3001525.

65 D. Tarn, C. E. Ashley, M. Xue, E. C. Carnes, J. I. Zink and C. J. Brinker, Mesoporous Silica Nanoparticle Nanocarriers: Biofunctionality and Biocompatibility, *Acc. Chem. Res.*, 2013, **46**, 792–801, 10.1021/ar3000986.

66 K. K. Cotí, M. E. Belowich, M. Liong, M. W. Ambrogio, Y. A. Lau, H. A. Khatib, J. I. Zink, N. M. Khashab, J. F. Stoddart, J. Fraser, M. E. Belowich, M. Liong, M. W. Ambrogio, Y. A. Lau, K. K. Cotı, H. A. Khatib, J. I. Zink, M. Khashab and J. F. Stoddart, Mechanised nanoparticles for drug delivery, *Nanoscale*, 2009, **1**, 16–39, 10.1039/b9nr00162j.

67 T. Shimada, K. Aoki, Y. Shinoda, T. Nakamura, N. Tokunaga, S. Inagaki and T. Hayashi, Functionalization on silica gel with allylsilanes. A new method of covalent attachment of organic functional groups on silica gel, *J. Am. Chem. Soc.*, 2003, **125**, 4688–4689, 10.1021/ja034691l.

68 T. Asefa and Z. Tao, Biocompatibility of Mesoporous Silica Nanoparticles, *Chem. Res. Toxicol.*, 2012, **25**, 2265–2284, 10.1021/tx300166u.

69 M. C. Gomes, Â. Cunha, T. Trindade and J. P. C. Tomé, The role of surface functionalization of silica nanoparticles for bioimaging, *J. Innov. Opt. Health Sci.*, 2016, **9**, 1–16, 10.1142/S1793545816300056.

70 N. Takahashi, H. Hata and K. Kuroda, Exfoliation of layered silicates through immobilization of imidazolium groups, *Chem. Mater.*, 2011, **23**, 266–273, 10.1021/cm102942s.

71 N. Moitra, S. Ichii, T. Kamei, K. Kanamori, Y. Zhu, K. Takeda, K. Nakanishi and T. Shimada, Surface functionalization of silica by Si-H activation of hydrosilanes, *J. Am. Chem. Soc.*, 2014, **136**, 11570–11573, 10.1021/ja504115d.

72 M. J. Sweetman, S. J. P. McInnes, R. B. Vasani, T. Guinan, A. Blencowe and N. H. Voelcker, Rapid, metal-free hydrosilanisation chemistry for porous silicon surface modification, *Chem. Commun.*, 2015, **51**, 10640–10643, 10.1039/c5cc02689j.

73 M. Nicola, L. M. Seymour, M. Aceto, E. Priola, R. Gobetto and A. Masic, Late production of Egyptian blue: synthesis from brass and its characteristics, *Archaeol. Anthropol. Sci.*, 2019, **11**, 5377–5392, 10.1007/s12520-019-00873-w.

74 G. Bains, A. B. Patel and V. Narayanaswami, Pyrene: A probe to study protein conformation and conformational changes, *Molecules*, 2011, **16**, 7909–7935, 10.3390/molecules16097909.

75 K. Ayyavoo and P. Velusamy, Pyrene based materials as fluorescent probes in chemical and biological fields, *New J. Chem.*, 2021, **45**, 10997–11017, 10.1039/d1nj00158b.

76 H. Maeda, H. Ishida, Y. Inoue, A. Merpuge, T. Maeda and K.

Mizuno, UV absorption and fluorescence properties of fused aromatic hydrocarbons having trimethylsilyl, trimethylgermyl, and trimethylstannyl groups, *Res. Chem. Intermed.*, 2009, **35**, 939–948, 10.1007/s11164-009-0076-y.

77 Y. Niko, S. Kawauchi, S. Otsu, K. Tokumaru and G. I. Konishi, Fluorescence enhancement of pyrene chromophores induced by alkyl groups through σ-π Conjugation: Systematic synthesis of primary, secondary, and tertiary alkylated pyrenes at the 1, 3, 6, and 8 positions and their photophysical properties, *J. Org. Chem.*, 2013, **78**, 3196–3207, 10.1021/jo400128c.

78 J. Ferguson, Absorption and fluorescence spectra of crystalline pyrene, *J. Chem. Phys.*, 1958, **28**, 765–768, 10.1063/1.1744267.

79 K. C. Park, C. Seo, G. Gupta, J. Kim and C. Y. Lee, Efficient Energy Transfer (EnT) in Pyrene- and Porphyrin-Based Mixed-Ligand Metal-Organic Frameworks, *ACS Appl. Mater. Interfaces*, 2017, **9**, 38670–38677, 10.1021/acsami.7b14135.

80 N. Y. C. Chu, K. Kawaoka and D. R. Kearns, Investigation of energy-transfer mechanisms in pyrene crystals, *J. Chem. Phys.*, 1971, **55**, 3059–3067, 10.1063/1.1676546.

81 G. F. Luo, W. H. Chen, Y. Liu, J. Zhang, S. X. Cheng, R. X. Zhuo and X. Z. Zhang, Charge-reversal plug gate nanovalves on peptide-functionalized mesoporous silica nanoparticles for targeted drug delivery, *J. Mater. Chem. B*, 2013, **1**, 5723–5732, 10.1039/c3tb20792g.

82 R. J. Hunter, *Zeta Potential in Colloid Science*, *Zeta Potential in Colloid Science*, Elsevier, 1981, 10.1016/C2013-0-07389-6.

83 B. Derjaguin and L. Landau, The theory of stability of highly charged lyophobic sols and coalescence of highly charged particles in electrolyte solutions, *Acta Physicochim. URSS*, 1941, **14**, 633–52.

84 E. J. W. Verwey, Theory of the stability of lyophobic colloids, *J. Phys. Chem.*, 1947, **51**, 631–636.

85 S. Sandoval, N. Mendez, J. G. Alfaro, J. Yang, S. Aschemeyer, A. Liberman, W. C. Trogler and A. C. Kummel, Quantification of endocytosis using a folate functionalized silica hollow nanoshell platform, *J. Biomed. Opt.*, 2015, **20**, 088003, 10.1117/1.jbo.20.8.088003.

86 M. Fernández, F. Javaid and V. Chudasama, Advances in targeting the folate receptor in the treatment/imaging of cancers, *Chem. Sci.*, 2018, **9**, 790–810, 10.1039/c7sc04004k.

87 A. Friedman, S. Claypool and R. Liu, The Smart Targeting of Nanoparticles, *Curr. Pharm. Des.*, 2013, **19**, 6315–6329, 10.2174/13816128113199990375.

88 A. F. Trindade, R. F. M. Frade, E. M. S. Maçôas, C. Graça, C. A. B. Rodrigues, J. M. G. Martinho and C. A. M. Afonso, "Click and go": simple and fast folic acid conjugation, *Org. Biomol. Chem.*, 2014, **12**, 3181–3190, 10.1039/C4OB00150H.

89 S. Mohapatra, S. K. Mallick, T. K. Maiti, S. K. Ghosh and P. Pramanik, Synthesis of highly stable folic acid conjugated magnetite nanoparticles for targeting cancer cells, *Nanotechnology*, , DOI:10.1088/0957-4484/18/38/385102, 10.1088/0957-4484/18/38/385102.

90 M. Xie, H. Shi, Z. Li, H. Shen, K. Ma, B. Li, S. Shen and Y. Jin, A multifunctional mesoporous silica nanocomposite for targeted delivery, controlled release of doxorubicin and bioimaging, *Colloids Surfaces B Biointerfaces*, 2013, **110**, 138–147, 10.1016/j.colsurfb.2013.04.009.

91 Z. Zhang, J. Jia, Y. Lai, Y. Ma, J. Weng and L. Sun, Conjugating folic acid to gold nanoparticles through glutathione for targeting and detecting cancer cells, *Bioorganic Med. Chem.*, 2010, **18**, 5528–5534, 10.1016/j.bmc.2010.06.045.

92 Y. K. Lee, Preparation and characterization of folic acid linked poly(L-glutamate) nanoparticles for cancer targeting, *Macromol. Res.*, 2006, **14**, 387–393, 10.1007/BF03219099.

93 E. Mornet, N. Carmoy, C. Lainé, L. Lemiègre, T. Le Gall, I. Laurent, R. Marianowski, C. Férec, P. Lehn, T. Benvegnu and T. Montier, Folate-equipped nanolipoplexes mediated efficient gene transfer into human epithelial cells, *Int. J. Mol. Sci.*, 2013, **14**, 1477–1501, 10.3390/ijms14011477.

94 F. A. Mann, P. Galonska, N. Herrmann and S. Kruss, Quantum defects as versatile anchors for carbon nanotube functionalization, *Nat. Protoc.*, 2022, **17**, 727–747, 10.1038/s41596-021-00663-6.

95 F. A. Mann, N. Herrmann, F. Opazo and S. Kruss, Quantum Defects as a Toolbox for the Covalent Functionalization of Carbon Nanotubes with Peptides and Proteins, *Angew. Chemie - Int. Ed.*, 2020, **59**, 17732–17738, 10.1002/anie.202003825.

96 M. Dinarvand, E. Neubert, D. Meyer, G. Selvaggio, F. A. Mann, L. Erpenbeck and S. Kruss, Near-Infrared Imaging of Serotonin Release from Cells with Fluorescent Nanosensors, *Nano Lett.*, 2019, **19**, 6604–6611, 10.1021/acs.nanolett.9b02865.

97 S. Elizarova, A. A. Chouaib, A. Shaib, B. Hill, F. Mann, N. Brose, S. Kruss and J. A. Daniel, A fluorescent nanosensor paint detects dopamine release at axonal varicosities with high spatiotemporal resolution, *Proc. Natl. Acad. Sci.*, 2022, **119**, 1–12, 10.1073/pnas.2202842119/-/DCSupplemental.Published.

98 S. Kruss, M. P. Landry, E. Vander Ende, B. M. A. A. Lima, N. F. Reuel, J. Zhang, J. Nelson, B. Mu, A. Hilmer and M. Strano, Neurotransmitter detection using corona phase molecular recognition on fluorescent single-walled carbon nanotube sensors., *J. Am. Chem. Soc.*, 2014, **136**, 713–724, 10.1021/ja410433b.

99 F. Mann, N. Herrmann, D. Meyer and S. Kruss, Tuning Selectivity of Fluorescent Carbon Nanotube-Based Neurotransmitter Sensors, *Sensors*, 2017, **17**, 1521, 10.3390/s17071521.

100 A. Spreinat, M. M. Dohmen, J. Lüttgens, N. Herrmann, L. F. Klepzig, R. Nißler, S. Weber, F. A. Mann, J. Lauth and S. Kruss, Quantum Defects in Fluorescent Carbon Nanotubes for Sensing and Mechanistic Studies, *J. Phys. Chem. C*, 2021, **125**, 18341–18351, 10.1021/ACS.JPCC.1C05432.

101 E. Polo and S. Kruss, Impact of Redox-Active Molecules on the Fluorescence of Polymer-Wrapped Carbon Nanotubes, *J. Phys. Chem. C*, 2016, **120**, 3061–3070, 10.1021/acs.jpcc.5b12183.

102 H. Jin, D. A. Heller, M. Kalbacova, J.-H. Kim, J. Zhang, A. A. Boghossian, N. Maheshri and M. S. Strano, Detection of single-molecule H2O2 signalling from epidermal growth factor receptor using fluorescent single-walled carbon nanotubes, *Nat. Nanotechnol.*, 2010, **5**, 302–309, 10.1038/nnano.2010.24.

103 N. M. Iverson, P. W. Barone, M. Shandell, L. J. Trudel, S. Sen, F. Sen, V. Ivanov, E. Atolia, E. Farias, T. P. McNicholas, N. Reuel, N. M. A. Parry, G. N. Wogan and M. S. Strano, In vivo biosensing via tissue-localizable near-infrared-fluorescent single-walled carbon nanotubes, *Nat. Nanotechnol.*, 2013, **8**, 873–880, 10.1038/nnano.2013.222.

104 J. H. Kim, C. R. Patra, J. R. Arkalgud, A. A. Boghossian, J. Zhang, J. H. Han, N. F. Reuel, J. H. Ahn, D. Mukhopadhyay and M. S. Strano, Single-molecule detection of H2O2 mediating angiogenic redox signaling on fluorescent single-walled carbon nanotube array, *ACS Nano*, 2011, **5**, 7848–7857, 10.1021/nn201904t.

105 J. Zhang, A. A. Boghossian, P. W. Barone, A. Rwei, J. H. Kim, D. Lin, D. A. Heller, A. J. Hilmer, N. Nair, N. F. Reuel and M. S. Strano, Single molecule detection of nitric oxide enabled by d(AT)15 DNA adsorbed to near infrared fluorescent single-walled carbon nanotubes, *J. Am. Chem. Soc.*, 2011, **133**, 567–581, 10.1021/ja1084942.

106 Z. W. Ulissi, F. Sen, X. Gong, S. Sen, N. Iverson, A. A. Boghossian, L. C. Godoy, G. N. Wogan, D. Mukhopadhyay and M. S. Strano, Spatiotemporal intracellular nitric oxide signaling captured using internalized, near-infrared fluorescent carbon nanotube nanosensors, *Nano Lett.*, 2014, **14**, 4887–4894, 10.1021/nl502338y.

107 J. H. Kim, D. A. Heller, H. Jin, P. W. Barone, C. Song, J. Zhang, L. J. Trudel, G. N. Wogan, S. R. Tannenbaum and M. S. Strano, The rational design of nitric oxide selectivity in single-walled carbon nanotube near-infrared fluorescence sensors for biological detection, *Nat. Chem.*, 2009, **1**, 473–481, 10.1038/nchem.332.

108 R. Nißler, A. T. Müller, F. Dohrman, L. Kurth, H. Li, E. G. Cosio, B. S. Flavel, J. P. Giraldo, A. Mithöfer and S. Kruss, Detection and Imaging of the Plant Pathogen Response by Near-Infrared Fluorescent Polyphenol Sensors, *Angew. Chemie - Int. Ed.*, 2022, **61**, 2022, 10.1002/anie.202108373.

109 Z. Yaari, Y. Yang, E. Apfelbaum, C. Cupo, A. H. Settle, Q. Cullen, W. Cai, K. L. Roche, D. A. Levine, M. Fleisher, L. Ramanathan, M. Zheng, A. Jagota and D. A. Heller, A perception-based nanosensor platform to detect cancer biomarkers, *Sci. Adv.*, 2021, **7**, 1–11, 10.1126/sciadv.abj0852.

110 R. M. Williams, C. Lee, T. V. Galassi, J. D. Harvey, R. Leicher, M. Sirenko, M. A. Dorso, J. Shah, N. Olvera, F. Dao, D. A. Levine and D. A. Heller, Noninvasive ovarian cancer biomarker detection via an optical nanosensor implant, *Sci. Adv.*, 2018, **4**, eaaq1090, 10.1126/sciadv.aaq1090.